

# Computer-Assisted Drug Discovery of a Novel Theobromine Derivative as an EGFR Protein-Targeted Apoptosis Inducer

Evolutionary Bioinformatics  
Volume 19: 1–16  
© The Author(s) 2023  
Article reuse guidelines:  
sagepub.com/journals-permissions  
DOI: 10.1177/11769343231217916



Ibrahim H Eissa<sup>1</sup>, Reda G Yousef<sup>1</sup>, Eslam B Elkaeed<sup>2</sup>, Aisha A Alsouk<sup>3</sup>, Dalal Z Husein<sup>4</sup>, Ibrahim M Ibrahim<sup>5</sup>, Hesham A El-Mahdy<sup>6</sup>, Hazem Elkady<sup>1</sup> and Ahmed M Metwaly<sup>7,8</sup> 

<sup>1</sup>Pharmaceutical Medicinal Chemistry & Drug Design Department, Faculty of Pharmacy (Boys), Al-Azhar University, Cairo, Egypt. <sup>2</sup>Department of Pharmaceutical Sciences, College of Pharmacy, AlMaarefa University, Riyadh, Saudi Arabia. <sup>3</sup>Department of Pharmaceutical Sciences, College of Pharmacy, Princess Nourah bint Abdulrahman University, Riyadh, Saudi Arabia. <sup>4</sup>Chemistry Department, Faculty of Science, New Valley University, El-Kharja, Egypt. <sup>5</sup>Biophysics Department, Faculty of Science, Cairo University, Cairo, Egypt. <sup>6</sup>Biochemistry and Molecular Biology Department, Faculty of Pharmacy, Al-Azhar University, Cairo, Egypt. <sup>7</sup>Pharmacognosy and Medicinal Plants Department, Faculty of Pharmacy (Boys), Al-Azhar University, Cairo, Egypt. <sup>8</sup>Biopharmaceutical Products Research Department, Genetic Engineering and Biotechnology Research Institute, City of Scientific Research and Technological Applications (SRTA-City), Alexandria, Egypt.

**ABSTRACT:** The overexpression of the Epidermal Growth Factor Receptor (EGFR) marks it as a pivotal target in cancer treatment, with the aim of reducing its proliferation and inducing apoptosis. This study aimed at the CADD of a new apoptotic EGFR inhibitor. The natural alkaloid, theobromine, was used as a starting point to obtain a new semisynthetic (di-ortho-chloro acetamide) derivative (**T-1-DOCA**). Firstly, **T-1-DOCA**'s total electron density, energy gap, reactivity indices, and electrostatic surface potential were determined by DFT calculations. Then, molecular docking studies were carried out to predict the potential of **T-1-DOCA** against wild and mutant EGFR proteins. **T-1-DOCA**'s correct binding was further confirmed by molecular dynamics (MD) over 100 ns, MM-GPSA, and PLIP experiments. In vitro, **T-1-DOCA** showed noticeable efficacy compared to erlotinib by suppressing EGFR<sup>WT</sup> and EGFR<sup>T790M</sup> with IC<sub>50</sub> values of 56.94 and 269.01 nM, respectively. **T-1-DOCA** inhibited also the proliferation of H1975 and HCT-116 malignant cell lines, exhibiting IC<sub>50</sub> values of 14.12 and 23.39 μM, with selectivity indices of 6.8 and 4.1, respectively, indicating its anticancer potential and general safety. The apoptotic effects of **T-1-DOCA** were indicated by flow cytometric analysis and were further confirmed through its potential to increase the levels of BAX, Casp3, and Casp9, and decrease Bcl-2 levels. In conclusion, **T-1-DOCA**, a new apoptotic EGFR inhibitor, was designed and evaluated both computationally and experimentally. The results suggest that **T-1-DOCA** is a promising candidate for further development as an anti-cancer drug.

**KEYWORDS:** Semi synthesis, EGFR inhibitors, MD simulation, ED, apoptosis, anti-proliferative, docking

**RECEIVED:** July 17, 2023. **ACCEPTED:** November 13, 2023.

**TYPE:** Original Research

**FUNDING:** The author(s) disclosed receipt of the following financial support for the research, authorship, and/or publication of this article: This research was funded by Princess Nourah bint Abdulrahman University Researchers Supporting Project number (PNURSP2023R116), Princess Nourah bint Abdulrahman University, Riyadh, Saudi Arabia. The authors extend their appreciation to the Research Center at AlMaarefa University for funding this work.

**DECLARATION OF CONFLICTING INTERESTS:** The author(s) declared no potential conflicts of interest with respect to the research, authorship, and/or publication of this article.

**CORRESPONDING AUTHORS:** Ibrahim H Eissa, Pharmaceutical Medicinal Chemistry & Drug Design Department, Faculty of Pharmacy (Boys), Al-Azhar University, Cairo 11884, Egypt. Email: Ibrahim.eissa@azhar.edu.eg

Ahmed M Metwaly, Pharmacognosy and Medicinal Plants Department, Faculty of Pharmacy (Boys), Al-Azhar University, Cairo 11884, Egypt. Email: ametwaly@azhar.edu.eg

## Introduction

Even with significant advancements, cancer treatment is still regarded as one of the most difficult medical issues. The burden of the cancer problem increasingly shifts to lower- and middle-income countries, reflecting the underlying socio-economic relationship.<sup>1</sup> Cancer, which claimed 9.6 million lives in 2018, is the second largest cause of death globally, according to the WHO. Over the next 20 years, there will likely be a 70% increase in the number of impacted people.<sup>2</sup>

The process of apoptosis is a vital cellular mechanism that responds to various oncogenic stresses, including uncontrolled proliferation or DNA damage, by eliminating damaged or potentially harmful cells.<sup>3</sup> This process is essential for preventing the development of cancer by removing cells that are at risk

of transformation.<sup>4</sup> In addition, apoptosis can suppress tumorigenesis by clearing oncogenic proteins and modulating cellular signaling pathways.<sup>5</sup> EGFR is a significant member of the protein kinases family that plays a critical role in apoptosis and is linked to cancer cells' elimination.<sup>6</sup> EGFR also contributes significantly to the development and progression of various types of carcinomas.<sup>7</sup> Overexpression of EGFR promotes cell proliferation, differentiation, and survival, and a high level of EGFR expression has been associated with a lower survival rate in many cancer types, making EGFR expression a powerful prognostic indicator.<sup>8</sup> One of the essential pathways that activated by the EGFR protein is the janus kinase, JAK, / signal transcription activators and transducers, STAT, pathway.<sup>9</sup> The JAK/STAT pathway has a pivotal role in mitosis simulation,



Creative Commons Non Commercial CC BY-NC: This article is distributed under the terms of the Creative Commons Attribution-NonCommercial 4.0 License (<https://creativecommons.org/licenses/by-nc/4.0/>) which permits non-commercial use, reproduction and distribution of the work without further permission provided the original work is attributed as specified on the SAGE and Open Access pages (<https://us.sagepub.com/en-us/nam/open-access-at-sage>).

causing cell proliferation and apoptosis inhibition.<sup>10</sup> Therefore, blocking its molecular function has significant antiproliferative and apoptotic effects<sup>11</sup> and could be considered a key approach in the development of novel treatments for cancer.<sup>12</sup>

In the field of drug discovery and development, the study of structure-activity relationships is an important factor in the creation of effective drugs.<sup>13-15</sup> Computer Assisted Drug Discovery (CADD) depends on the relationships between a drug's chemical structure and its biological activity that could be applied to optimize drug-likeness, pharmacokinetics, and pharmacodynamics.<sup>16</sup> CADD has become an increasingly important tool in the pharmaceutical industry, where it is used to speed up the drug discovery process and reduce costs.<sup>17</sup>

Over the years, a range of CADD applications have been developed. These include molecular and drug design,<sup>18,19</sup> docking simulations,<sup>20</sup> ligand-based approaches such as pharmacophore assessment,<sup>21</sup> structure similarity,<sup>22</sup> and ADMET<sup>23</sup> are also widely used. Other computational chemistry techniques include DFT, which is used to study the electronic structure of molecules.<sup>24</sup> Molecular dynamics (MD) simulations are a powerful CADD tool for investigating the dynamic behavior, energetic and structural changes of proteins at the atomic level.<sup>25</sup> These simulations provide an opportunity to explore protein-ligand interactions offering precise descriptions of the conformational changes induced by ligand binding in a protein.<sup>26</sup> Therefore, MD simulations are a valuable approach for studying protein dynamics and ligand binding mechanisms.<sup>27</sup> CADD involves the use of software employing a variety of techniques to study the interactions between potential drugs and biomolecules.

The need for new EGFR inhibitors arises from the challenge of overcoming resistance that cancer cells develop to current drugs.<sup>28</sup> This resistance often stems from mutations in the EGFR gene<sup>29</sup> or activation of alternative signaling pathways.<sup>30</sup> Additionally, novel inhibitors, particularly those derived from natural compounds like our lead drug, hold the promise of providing improved safety profiles with fewer side effects compared to existing medications.<sup>31-33</sup> Many EGFR inhibitors were discovered and reported to have promising activity in the clinical treatment of cancer.<sup>34</sup> There are 4 essential pharmacophoric features that EGFR inhibitors share, allowing them to effectively bind to diverse pockets within the ATP binding site. Firstly, these inhibitors possess a flat heteroaromatic ring/rings that occupy the adenine binding pocket.<sup>35</sup> Secondly, a terminal hydrophobic head is present, which is responsible for binding to hydrophobic region I. The third feature is an NH spacer that can form essential hydrogen bonding interactions with the amino acid residues inside the linker region.<sup>36</sup> Lastly, a hydrophobic tail is included, which is directed into the hydrophobic region II.<sup>37,38</sup> The above-mentioned features, as shown in Figure 1, are crucial for the design of effective EGFR inhibitors and for understanding their binding mechanism.

Figure 1 illustrates these features in several EGFR inhibitors. Erlotinib **I** was approved as a monotherapy for the treatment

of NSCLC. Then, its combination with gemcitabine was approved for the treatment of advanced pancreatic cancer.<sup>39,40</sup> Afatinib **II** belongs to the second-generation irreversible EGFR blocker that was approved for the treatment of NSCLC in EGFR mutation-positive adult patients.<sup>41</sup> Further investigations revealed its potential against breast cancer.<sup>42</sup> Avitinib **III**, third generation EGFR inhibitor.

Human beings have always depended on nature for their basic needs, including medicinal treatments, nourishing food, and cosmetic products, both in the past and in the present.<sup>43,44</sup> Our team utilized the natural sources to present compound **IV**, theobromine derivative, as a promising EGFR inhibitor. A such compound showed good anti-proliferative activity against A549 and HCT-116 cell lines with high levels of selectivity.<sup>45</sup> Furthermore, another theobromine derivative **V** was reported by our team. A such compound inhibited EGFR<sup>WT</sup> and EGFR<sup>T790M</sup> with good cytotoxicity against A549 and HCT-116 cells.<sup>46</sup> Moreover, a xanthine-oxime hybrid **VI** was reported to possess promising antiproliferative and EGFR inhibitory activity. A such compound positively affected the apoptotic pathway through the modulation of caspases and Bax-Bcl-2 levels.<sup>47</sup>

### Rationale

Compounds **VI**, **V**, and **VI** were employed as primary compounds in the search for a novel inhibitor of EGFR. These compounds are derived from a naturally existing xanthine structure. Figure 2 demonstrates that the modified compound (**T-1-DOCA**) incorporates the xanthine structure in order to occupy the adenine binding pocket. The xanthine structure is well-known in the biological system as it occurs naturally. Additionally, the acetamide structure was utilized as a connecting component. Furthermore, the 2,6-dichlorobenzene was utilized as a hydrophobic component to occupy the hydrophobic region I. By incorporating the 2,6-dichlorobenzene moiety, the hydrophobicity of the synthesized compound could potentially be increased, thereby promoting the formation of hydrophobic interactions. Additionally, the presence of 2 chloro groups at the ortho position of the amide moiety might exert a steric effect, preventing the hydrolysis of the amide moiety by various amidases present in the physiological system.

Moreover, the theobromine moiety in **T-1-DOCA** features 2 methyl groups located at the 3- and 7-positions. These methyl groups serve to occupy the hydrophobic region II, as illustrated in Figure 2. The binding mode of the synthesized compound has confirmed the effectiveness of the design, as each specific feature successfully occupies its intended target pocket within the ATP binding site.

This article reports on the ongoing research of our team to discover potential anticancer agents that target EGFR protein.<sup>45,48-52</sup> The focus of this paper is to introduce a newly synthesized compound, **T-1-DOCA**, which exhibits promising *in silico* and *in vitro* anticancer properties. This novel

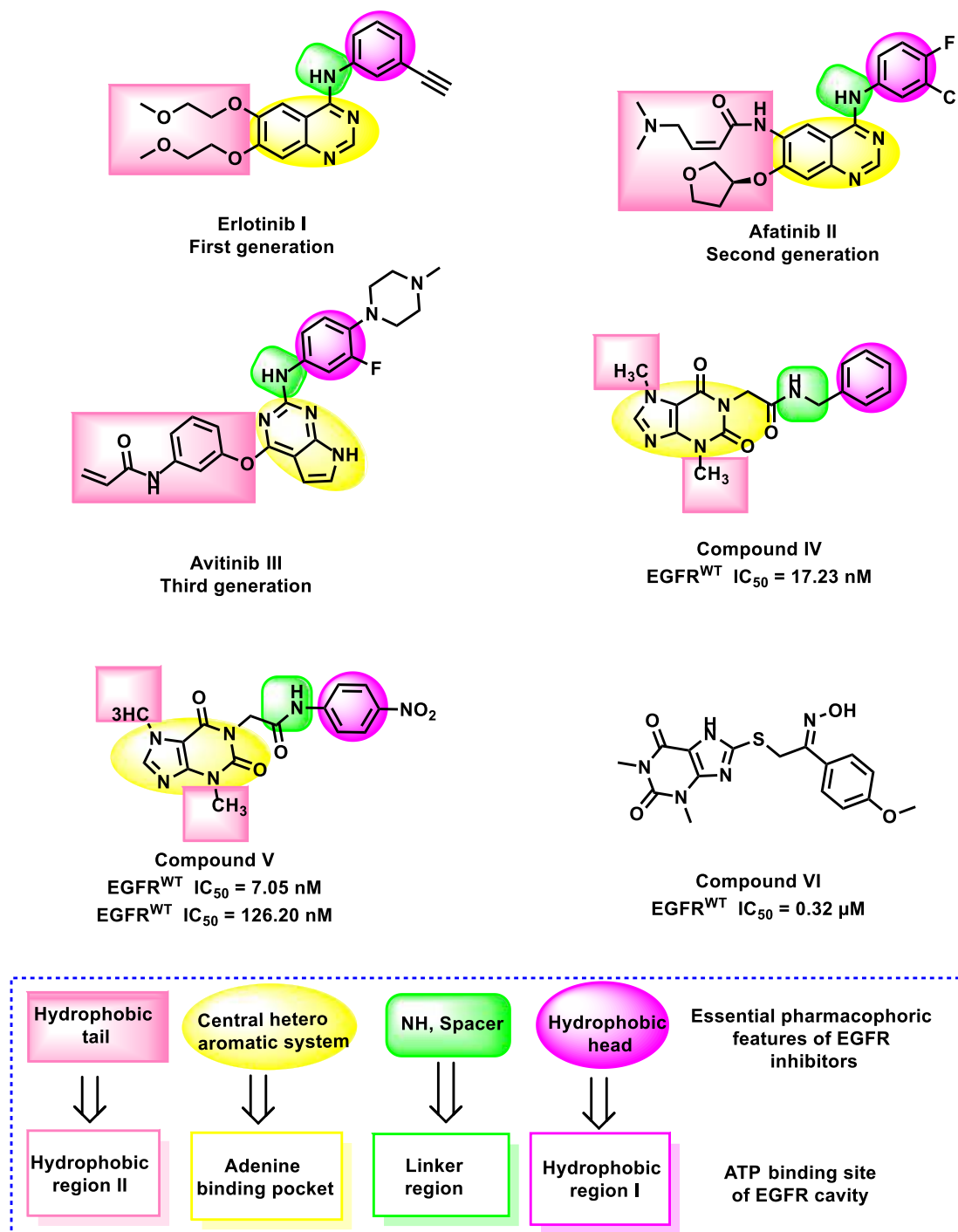


**Figure 1.** The crucial 4 pharmacophoric features of EGFR inhibitor drugs.

compound was specifically designed and synthesized to target EGFR protein and represents a potential lead compound in the development of new anticancer agents.

## Results and Discussions

### Dft

*Geometry optimization and Mulliken charge.* To clarify the correlation between the chemical system's structure, reactivity, and selectivity of active sites of **T-1-DOCA**, DFT-based analyses

have been carried out. B3LYP /6-311++G(d, p) level has been used for optimization in order to study the electronic structure, stability, and electronic characteristics of **T-1-DOCA**. As illustrated in Figure 3A, the generated bond in the synthesis of **T-1-DOCA** was determined to be 1.476 Å. With 38 atoms, 196 electrons, and a total ground state (TE) of -54410.6 eV, **T-1-DOCA** is a singlet neutral system. With a dipole moment value of 4.88 Debye, **T-1-DOCA**'s structure was predicted to be polarizable, which led to significant charge transfer and expected reasonable reactivity.

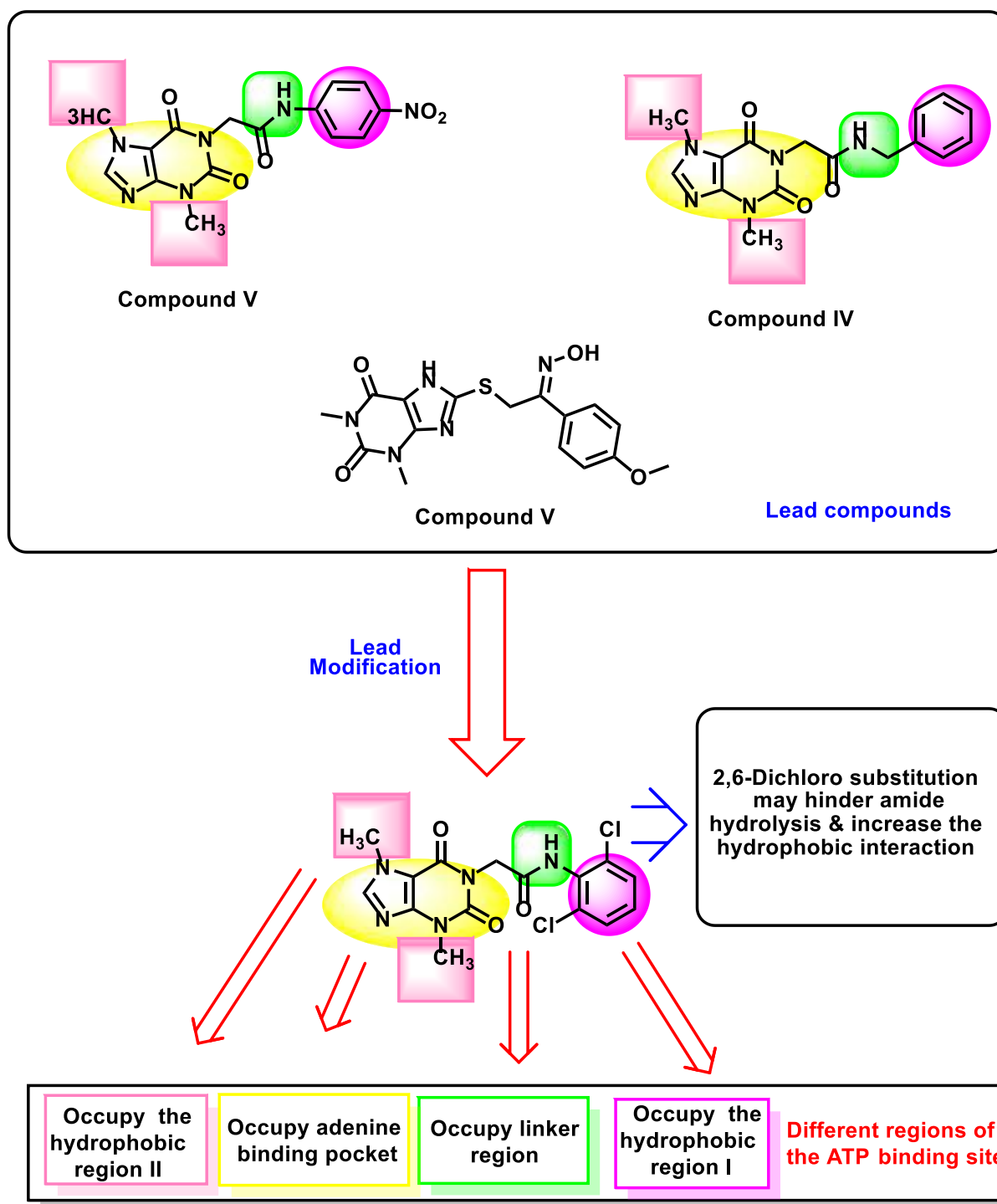


**Figure 2.** The design rationale of T-1-DOCA.

The Mulliken charge analysis is another sign of charge transfer and polarizability. It is shown in color scale in Figure 3B and the direction of the dipole moment is illustrated. The charge distribution within T-1-DOCA indicates that the greatest negative charge is found on the atoms in red color, while the most positive charge is found on the atoms in green color. According to Figure 3B, there is a significant charge transfer that supports T-1-DOCA's biological reactivity.

*Frontier molecular orbital (FMO) analysis.* Figure 4 shows the results of the FMOs study for T-1-DOCA utilizing "the B3LYP/6-31G level." Table 1 lists the estimated values of the developed drug's HOMO, LUMO, energy gap, and other important variables. Qualitative information regarding the electronic excitation properties of T-1-DOCA can be provided by the FMO study. The FMO study also offers qualitative data regarding T-1-DOCA's affinity to bind with the

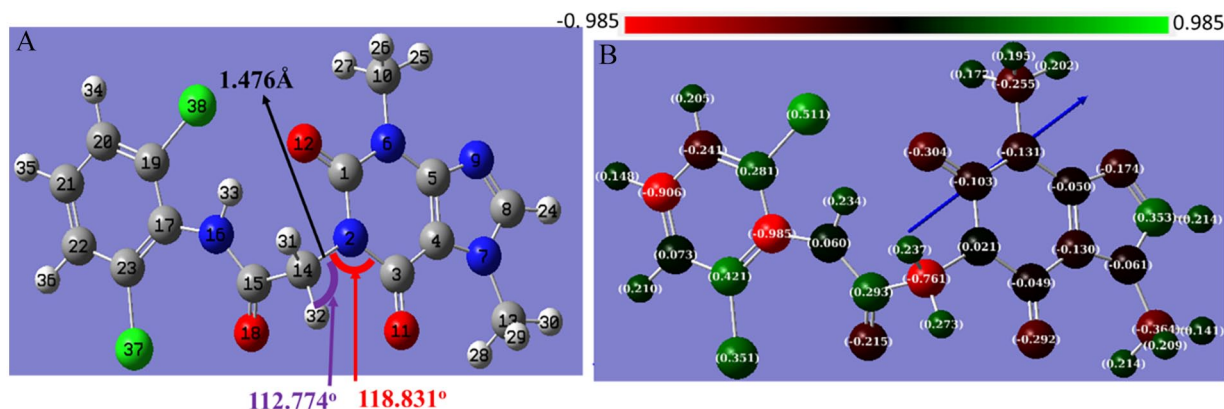


**Figure 3.** T-1-DOCA's fully optimized chemical structure (A), and the Mulliken charge (B) at B3LYB/6-311G++(d,p) level.

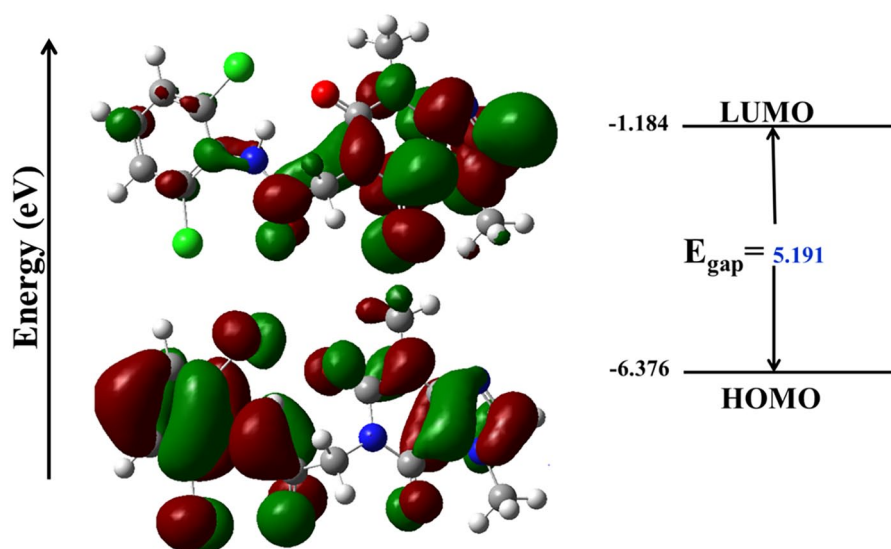


**Figure 4.** T-1-DOCA's FMO and energy levels at B3LYB/6-311G++(d,p) level.

**Table 1.** T-1-DOCA's reactivity indices and energetic parameters.

IP	EA	$\mu$ (EV)	$\chi$ (EV)	$\eta$ (EV)	$\sigma$ (EV)	$\omega$ (EV)	DM (DEBYE)	TE (EV)	$\Delta N_{MAX}$	$\Delta E$ (EV)
-6.376	-1.184	-3.780	3.780	2.596	0.385	18.544	4.777	-54410.6	1.456	-18.544

target. The computed parameters influence the strength of nonbonding forces between **T-1-DOCA** and the target, such as hydrophilic interactions and hydrogen bonding. Additionally, the stability of **T-1-DOCA** can be affirmed by the negative values of the HOMO and LUMO energies,  $E_{HOMO}$  and  $E_{LUMO}$ , respectively. The gap ( $E_{gap}$ ) between the HOMO and LUMO orbitals of **T-1-DOCA** reveals details about its kinetic stability and chemical reactivity. Theoretically computed  $E_{gap}$  value in Figure 4 implies the high reactivity of **T-1-DOCA** and a high degree of charge transfer from the donor to the acceptor.<sup>53</sup> According to Figure 2, the acetamide terminal of **T-1-DOCA** contains the majority of the HOMO density and the small density is localized on the purine ring. In the LUMO map, the purine moiety contains the majority of density.

These findings support the idea that intermolecular charge transfer could occur easily. According to Table 1, **T-1-DOCA** exhibits a strong binding affinity according to the electronic ionization potential (IP) and electron affinity (EA) values, which may be a result of its smaller  $E_{gap}$ . The greater affinity to donate electrons to the nearby chemical system is inversely proportional to the smaller value of  $E_{gap}$  or band difference.

*Descriptors of chemical reactivity and total density of state (TDOS).* In FMO analysis, Koopman's theorem was applied to determine the molecular electronic properties and global reactivity receptors of **T-1-DOCA**, including ionization potential (IP), electron affinity (EA), electrophilicity ( $\omega$ ),

chemical hardness ( $\eta$ ), maximal charge acceptance ( $N_{\max}$ ), chemical electronegativity ( $\chi$ ) and global softness ( $\delta$ ). According to Table 1, TDOS's high softness ( $\sigma$ ) value and low values of electrophilicity ( $\omega$ ), hardness ( $\eta$ ), and ionization potential (IP) values all indicate a high degree of reactivity. The stability of the system to gain an additional charge  $\Delta N$  from the nearby chemical system or target is determined by the magnitude of  $\omega$ , which is similar to the magnitude of  $\eta$  and IP.<sup>54</sup> The results of the global reactivity are consistent with the earlier discussions.

Figure 5 displays the relative spectrum after analysis of the "total density distribution function, TDOS." In the situation that the FMO analysis is unable to provide a complete description, the TDOS spectrum is a crucial tool for locating the maximum density. Virtual orbitals above the LUMO orbital, according to the TDOS study in Figure 5, have the highest electronic density.

*Electrostatic potential maps (ESP).* The active binding sites and hydrogen bonds (H-Bs) with the target are determined by the molecular electrostatic potential (ESP), which is a representation of the 3D surface charge distribution (both positive and negative) over the chemical structure of **T-1-DOCA**. The ESP surface maps, shown in Figure 6, were generated using the 6-311G++(d,p) basis set in DFT/B3LYP. The oxygen atoms of **T-1-DOCA** have negative chemical potential (red areas) and represent the electron-rich locations that encourage

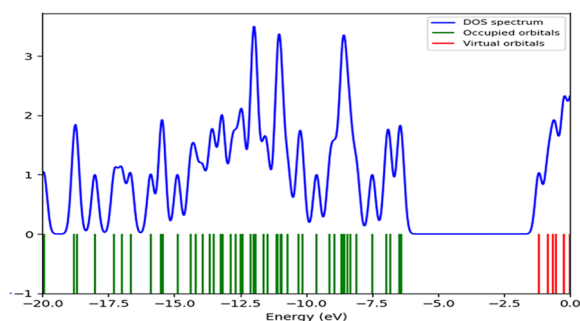


**Figure 5.** T-1-DOCA's FMO and TDOS at B3LYP/6-311++G(d,p).

electrophilic attacks. The nucleophilic attacks are localized over the hydrogen atoms and colored with the blue batches. These blue batches can act as a donor in H-Bs, whereas the oxygenated groups can act as acceptors. The yellowish-green region over the phenol ring has the potential to interact hydrophobically with the target. These outcomes supported all prior discussions and demonstrated **T-1-DOCA**'s reactivity as a potent anticancer inhibitor.

### *Molecular docking against EGFR proteins*

MOE protocol was applied for **T-1-DOCA** against wild (EGFR<sup>WT</sup>) and mutant (EGFR<sup>T790M</sup>) types of EGFR kinase (PDB: 4HJO and 3W2O, respectively). The obtained results were visualized using Discovery Studio 4.0. The docking poses of erlotinib and TAK-285, as co-crystallized ligands of wild and mutant EGFR, were matched with the reported findings<sup>55,56</sup> as presented in Figure 7.

**T-1-DOCA** exhibited the correct binding mode inside EGFR<sup>WT</sup> and EGFR<sup>T790M</sup> active sites. The 3,7-dimethyl-2,6-dioxo-2,3,6,7-tetrahydro-1H-purine arm was incorporated in key H-B interactions with Met769 and Met793 of the adenine pocket of EGFR<sup>WT</sup> and EGFR<sup>T790M</sup>, respectively. Furthermore, the 2,6-dichlorophenyl moiety of **T-1-DOCA** was buried in the conserved hydrophobic regions of both wild and mutant pockets. This was achieved through hydrophobic bonds (H-I) with Leu820, Ala719, Lys721, Ile720, and Val702 for EGFR<sup>WT</sup> (Figure 8A and B) and with Met790 and Lys745 for EGFR<sup>T790M</sup> (Figure 8C and D).

### *MD simulations*

The analysis of 100 ns of the MD production run shows that the EGFR-**T-1-DOCA** complex exhibits a stable and steady behavior. Interestingly, the RMSD plot (Figure 9A) indicates a very stable average for both the EGFR protein (blue) and the EGFR-**T-1-DOCA** complex (green) with values around 1.8 Å for the whole duration of the simulation (100 ns). Moreover, The RMSD of **T-1-DOCA** (red curve) exhibits stable

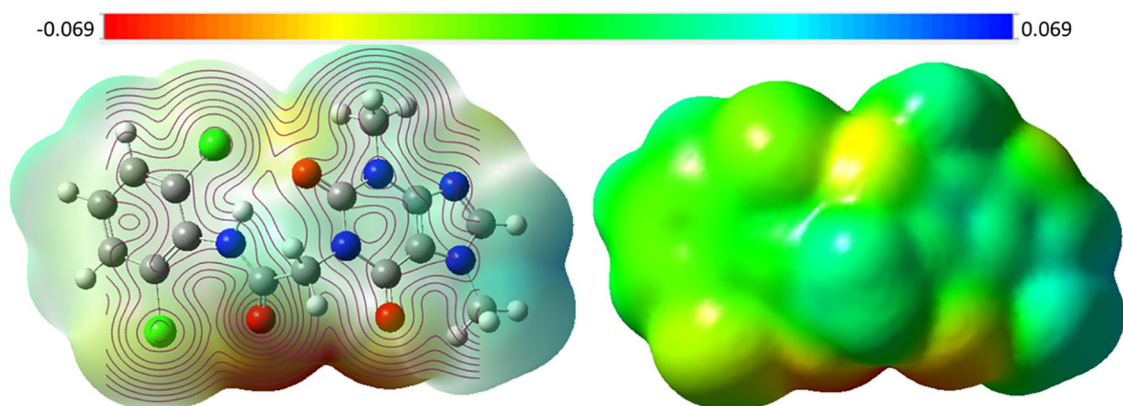


**Figure 6.** T-1-DOCA's ESP at the 6-311G++(d,p) level.

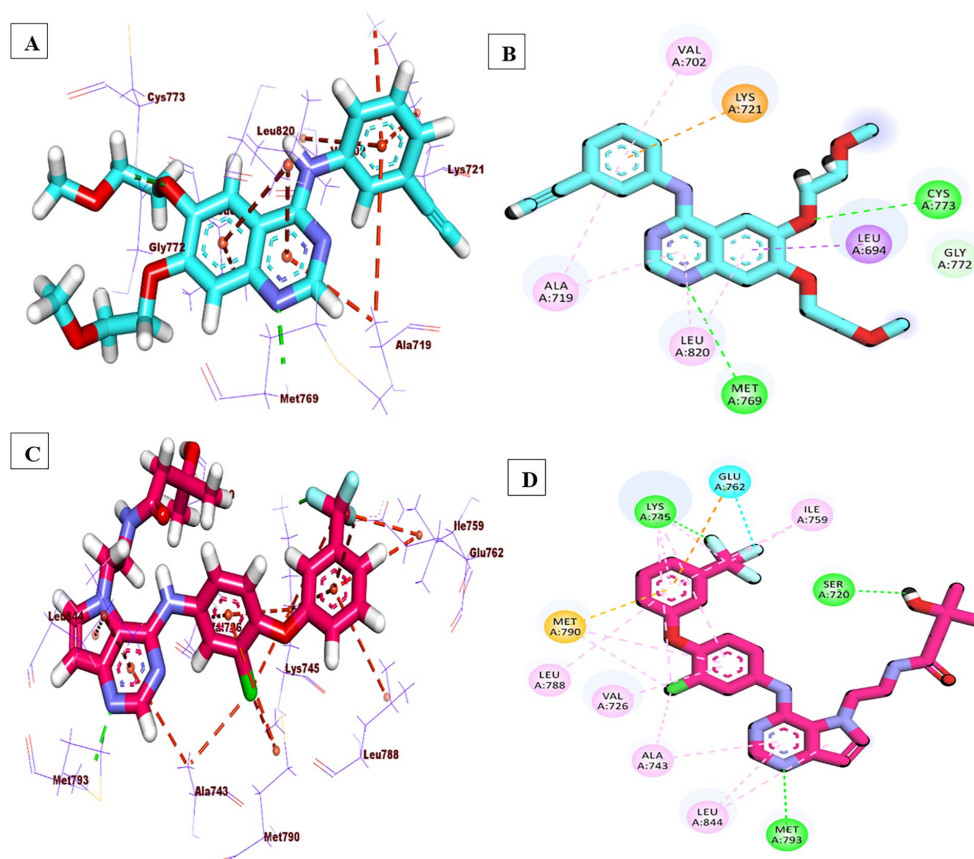


**Figure 7.** (A and B) 3D & 2D representations of erlotinib, (C and D) 3D & 2D representations of TAK-285.

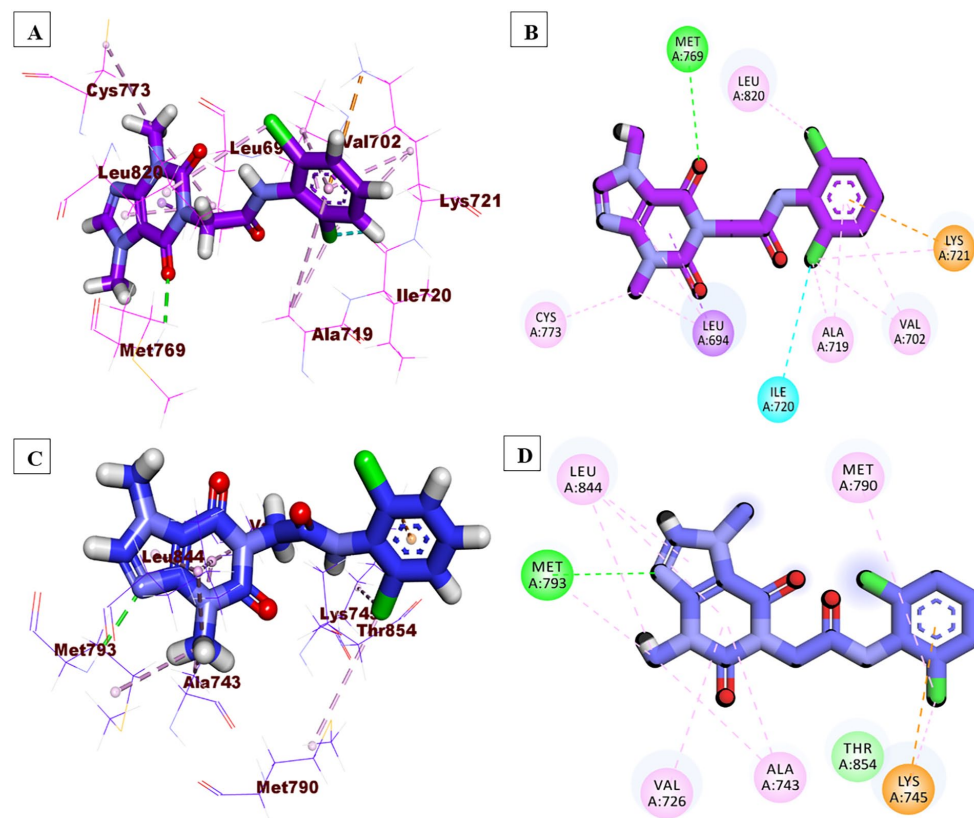


**Figure 8.** (A and B) 3D & 2D of T-1-DOCA inside EGFR<sup>WT</sup>, (C and D) 3D & 2D of T-1-DOCA inside EGFR<sup>T790M</sup>.

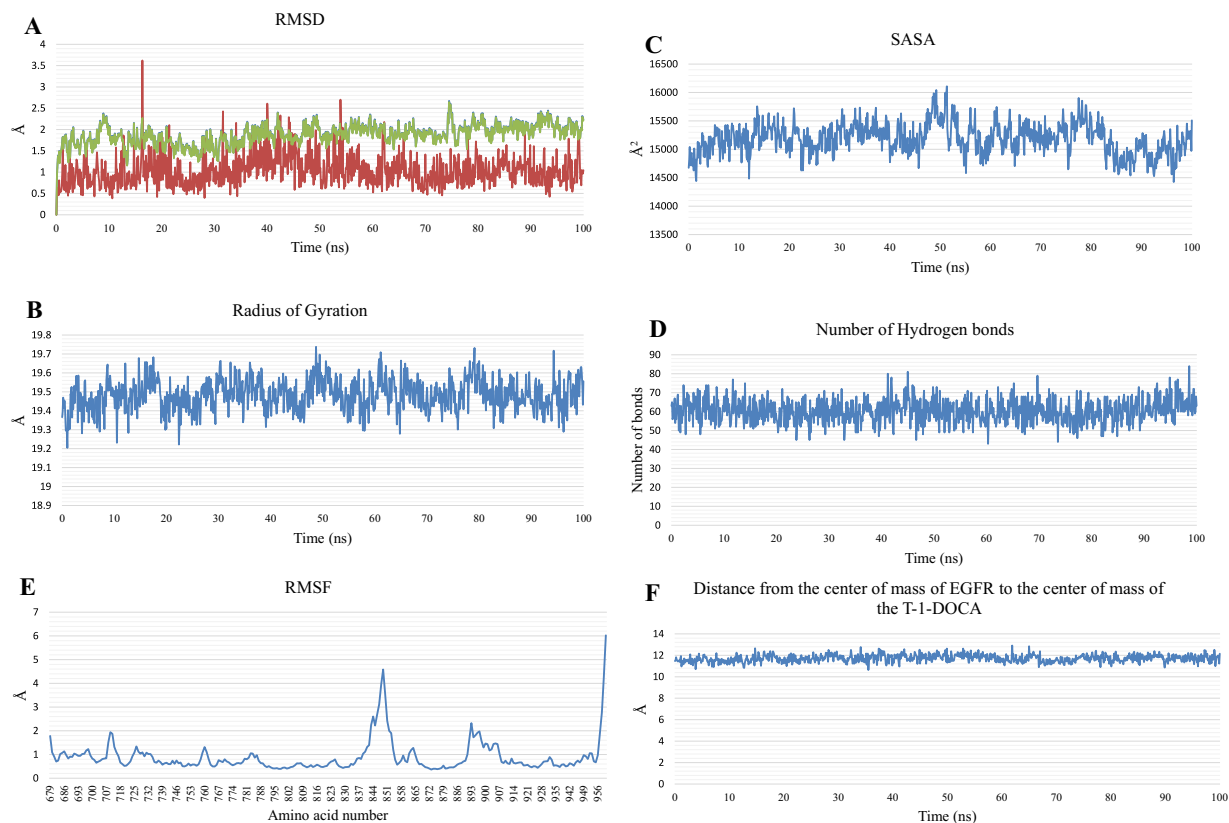


**Figure 9.** (A) RMSD, (B) Ro G, (C) SASA, (D) H-Bs, (E) RMSF, and (F) Center of Mass distance through the EGFR-T-1-DOCA complex.

fluctuations with only an average of  $1.03 \text{ \AA}$ . Additionally, the RoG (Figure 9B) and SASA (Figure 9C) values show stable average values around  $19.48 \text{ \AA}$  and  $15184 \text{ \AA}^2$  and SASA (Figure 9C), respectively. Moreover, Figure 9D of H-Bs reveals a strong bonding with a steady variation (average of 60 bonds). The RMSF plot (Figure 9E) shows relatively a low variation level ( $<2 \text{ \AA}$ ) for the included amino acids, except for the K843:P853, and the C-terminal, which reach a maximum of  $4.5 \text{ \AA}$ , and  $6 \text{ \AA}$ , respectively. Interestingly, throughout the 100 ns of the simulation, T-1-DOCA maintained a stable distance from the EGFR's center of mass with an average of  $11.7 \text{ \AA}$ . These outputs demonstrate the stability of the binding through the EGFR-T-1-DOCA complex.

#### MM-GBSA of the T-1-DOCA \_EGFR complex

The binding free energy analysis conducted using MM-GBSA (depicted in Figure 10) showcases the various factors involved in the binding process. For T-1-DOCA, the average binding free energy is calculated to be  $-32.63 \text{ kcal/mol}$ . Specifically, the average values for van der Waals and electrostatic interactions are approximately  $-43.91$  and  $-38.71 \text{ kcal/mol}$ , respectively. These values shed light on the strengths of the different types of interactions between T-1-DOCA and the receptor.

Additionally, Figure 11 presents a decomposition analysis that identifies the specific amino acids in close proximity to

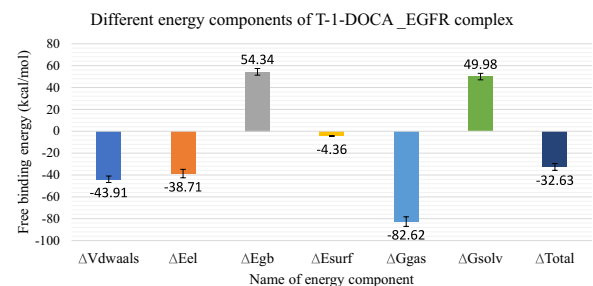


**Figure 10.** MM-GBSA of the T-1-DOCA \_EGFR complex. Bars represent the standard deviations.

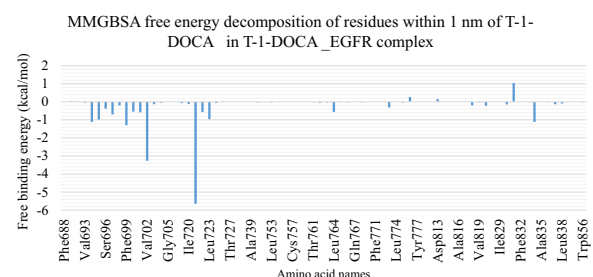


**Figure 11.** Binding energy decomposition of the T-1-DOCA \_EGFR complex.

T-1-DOCA. This analysis highlights the amino acids that play a significant role in the interaction and make the most substantial contributions to the binding process.

**Table 2.** PLIP analysis of **T-1-DOCA** and the EGFR protein.

CLUSTER NUMBER	HALOGEN BONDS	AMINO ACIDS	H-IS	AMINO ACIDS	H-BS	AMINO ACIDS
C1	1	Asp831	2	Lys721 - Leu834	1	Lys721
C2	1	Asp831	2	Phe699 - Leu723	1	Lys721
C3	1	Asp831	2	Lys721 - Leu723	1	Lys721

The amino acids that contribute with a value greater (less) than  $-1$  kcal.mol<sup>-1</sup> are Leu694 ( $-1.11$  kcal.mol<sup>-1</sup>), Phe699 ( $-1.29$  kcal.mol<sup>-1</sup>), Val702 ( $-3.26$  kcal.mol<sup>-1</sup>), Lys721 ( $-5.64$  kcal.mol<sup>-1</sup>), and Leu834 ( $-1.11$  kcal.mol<sup>-1</sup>). Interestingly, there is one amino acid (Asp831) that has a positive binding contribution with an average of ( $+1.03$  kcal.mol<sup>-1</sup>).

#### PLIP of the *T-1-DOCA*\_EGFR complex

To obtain representative frames for each cluster, the trajectory of the **T-1-DOCA**\_EGFR complex was subjected to clustering. The number of clusters was automatically determined using the elbow method, as explained in the methodology section, which resulted in 3 clusters. The PLIP website was then utilized to identify and quantify the interactions between **T-1-DOCA** and the EGFR protein for each representative frame, as detailed in Table 2.

Among the 3 representative frames, the amino acids Lys721 and Asp831 were found to be the most frequently occurring. Lys721 formed a hydrogen bond (H-B) while Asp831 formed a halogen bond with the chloride atom. Additionally, two hydrogen-ion interactions (H-Is) were observed in each of the 3 cluster representatives. These findings are in line with the minor difference between the electrostatic and van der Waals energy values obtained from the MM-GBSA analysis.

Furthermore, the PLIP analysis not only provided information on the types and numbers of interactions, but also generated a .pse file, enabling visualization of the three-dimensional conformation of **T-1-DOCA** and its interactions with the protein. Figure 12 illustrates this visual representation.

The ATP binding site of EGFR is part of the tyrosine kinase domain of the EGFR, which is responsible for the receptor's intracellular signaling activity.

While the ATP binding site is naturally competitive for any molecule, a molecule's higher affinity primarily hinges on how well each of its pharmacophores can interact with specific amino acids within designated sub-pockets. In our study, we crafted **T-1-DOCA** with various distinct pharmacophores, each possessing specific physical and chemical properties that facilitated its proper alignment, binding, and extended stability within its respective sub-pocket. This inherent stability of each pharmacophore within its designated sub-pocket contributed to the compound's remarkable affinity, stability, and intrinsic activity against the EGFR protein.

Interestingly, the docking studies affirmed **T-1-DOCA**'s strong affinity for the EGFR binding site. Specifically, the

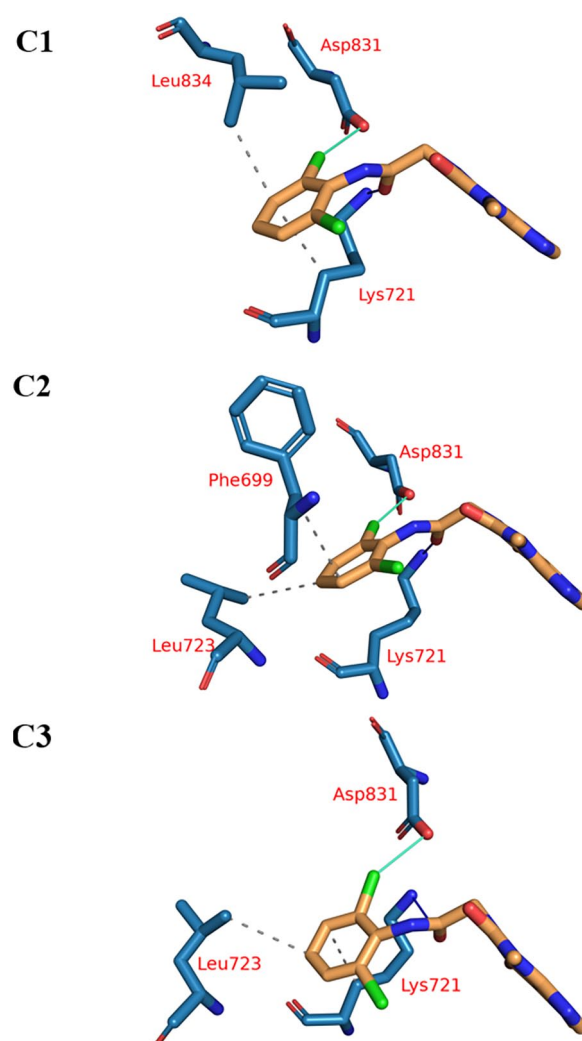


**Figure 12.** PLIP for the obtained 3 cluster representatives. Halogen bonds: green solid lines, H-I: dashed gray line, H-B: Blue solid line, amino acids: blue sticks, and **T-1-DOCA** and the EGFR protein: orange sticks representation.

3,7-dimethyl-2,6-dioxo-2,3,6,7-tetrahydro-1H-purine moiety displayed notable stability via hydrogen bonding with key amino acids (Met769 and Met793) of EGFRWT and EGFR790M, respectively. Simultaneously, the 2,6-dichlorophenyl segment snugly occupied the hydrophobic pocket I of the active site, engaging in numerous hydrophobic interactions. The linker group provided sufficient distance for the 2,6-dichlorophenyl segment to effectively utilize hydrophobic pocket I. To validate **T-1-DOCA**'s stability in the EGFR active site, MD simulation studies were conducted.

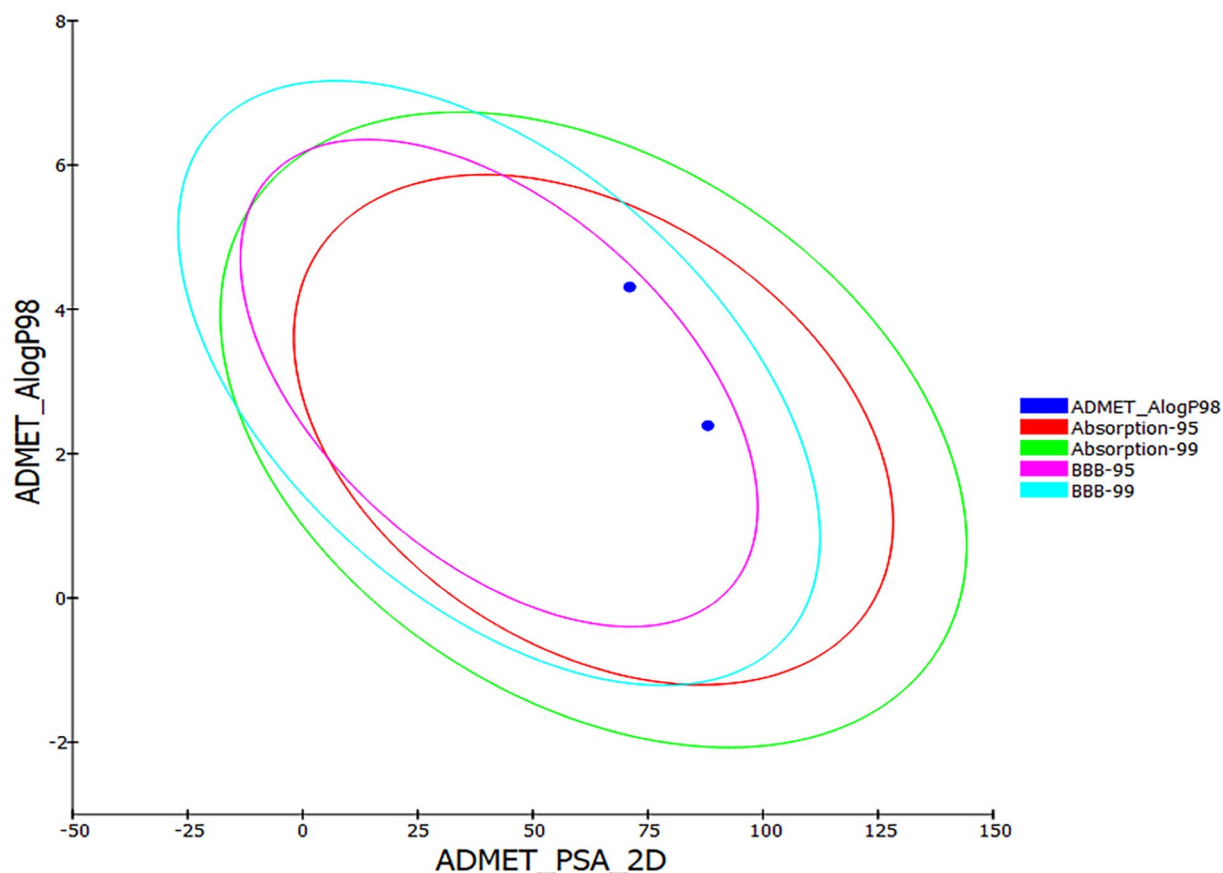


**Figure 13.** Computationally predicted ADMET parameters for **T-1-DOCA** and erlotinib.

**Table 3.** ADMET profile (computational) for **T-1-DOCA** and erlotinib.

COMP.	BBB-L	A.S	HEPATOTOXICITY	I.A	CYP-2D6	PPB.L
<b>T-1-DOCA</b>	Low	Moderate	Non-toxic	Good	False	<90%
Erlotinib	High		Toxic			>90%

These results demonstrated the compound's consistent presence in the active pocket throughout 100 ns, confirming ample time for intrinsic activity to occur. Taken together, from design through docking, MD simulation and the experimental studies, it is evident that **T-1-DOCA** exhibits commendable affinity, stability, and intrinsic activity against EGFR.

#### *ADMET profiling study*

The approval of a new medication relies on assessing both its pharmacokinetic properties and biological activity.<sup>57</sup> Thus, it is essential to evaluate the pharmacokinetic characteristics of a new compound early in the drug development process to prevent any potential delays in approval or late withdrawal.<sup>58</sup> To achieve this, ADMET parameters of **T-1-DOCA** were determined using Discovery Studio 4.0 computational tools (Figure 13 and Table 3). When compared to erlotinib, the ADMET results showed a higher degree of similarity showing

moderate and good levels of aqueous solubility (A.S) and intestinal absorption (I.A), respectively. Also, the inhibition of CYP-2D6 was expected to be absent in both compounds. Interestingly, the results indicated that **T-1-DOCA** was better than erlotinib in 3 parameters as it exhibited a low level of hepatotoxicity, a poor ability to penetrate the blood-brain barrier (BBB-L) and a plasma protein binding (PPB.L) ability of <90%.

#### *Lipinski's and Veber's rules violation*

If a molecule adheres to at least 3 of Lipinski's rules (H bond donors  $\leq 5$ , H bond acceptors  $\leq 10$ , molecular weight  $< 500$ , and  $\log P < 5$ ), it is more likely to have improved oral absorption. Compounds that deviate from more than one of these criteria are unlikely to exhibit high bioavailability. Additionally, reduced molecular flexibility, as indicated by a lower number of rotatable bonds, along with a smaller polar surface area, are key

**Table 4.** Physicochemical properties of **T-1-DOCA** according to Lipinski's and Veber's Rules.

COMPOUND	LIPINSKI'S RULE OF 5				VEBER'S RULE		VIOLATION OF LIPINSKI'S AND VEBER'S RULES
	LOG P	MOLE. WT.	HBD	HBA	NUMBER OF ROTATABLE BONDS	TPSA	
<b>T-1-DOCA</b>	1.87	382.20	1	8	3	87.54	0

**Table 5.** In silico toxicity studies of **T-1-DOCA** and erlotinib.

TOXICITY MODEL	T-1-DOCA	ERLOTINIB
Ames mutagenicity	No mutagenicity	
FDA Male-rats Carcinogenicity	No carcinogenicity	
Mouse Carcinogenic Potency TD <sub>50</sub>	36.1933 mg.kg <sup>-1</sup> .day <sup>-1</sup>	8.05746 mg.kg <sup>-1</sup> .day <sup>-1</sup>
Male-rats -Maximum Tolerated Feeding Dose	0.0284396 g.kg <sup>-1</sup>	0.0827884 g.kg <sup>-1</sup>
Male-rats -Oral LD <sub>50</sub>	1.11766 g.kg <sup>-1</sup>	0.662169 g.kg <sup>-1</sup>
Male-rats -Chronic LOAEL	0.0105009 g.kg <sup>-1</sup>	0.0359487 g.kg <sup>-1</sup>
Ocular irritation	Mildly irritant	
Dermal irritation	None irritant	

indicators of favorable oral bioavailability.<sup>59</sup> Also, compounds featuring 10 or fewer rotatable bonds and a polar surface area of 140 Å or less tend to have a heightened likelihood of good oral bioavailability.<sup>57,59</sup> In the case of **T-1-DOCA**, the results demonstrated compliance with both Lipinski's and Veber's rules (Table 4). This suggests a potential for high oral bioavailability of the synthesized compound.

#### *In silico toxicity studies*

Ensuring adequate toxicity estimation in the early stages of drug development is critical to minimizing drug approval failures.<sup>60</sup> However, using in vitro and in vivo methods can be ethically restricted, expensive, and time-consuming.<sup>61</sup> Therefore, the use of in silico techniques in toxicity prediction is necessary to avoid these challenges. In this study, the toxicity of **T-1-DOCA** was estimated using 8 toxicity models in the Discovery studio program, compared to erlotinib. Fortunately, the results showed that **T-1-DOCA** had safe values in all of the models run (Table 5). By using in silico techniques to predict toxicity, researchers can reduce the time and cost involved in drug development while still ensuring that the drug is safe and effective for human use

#### *Chemistry*

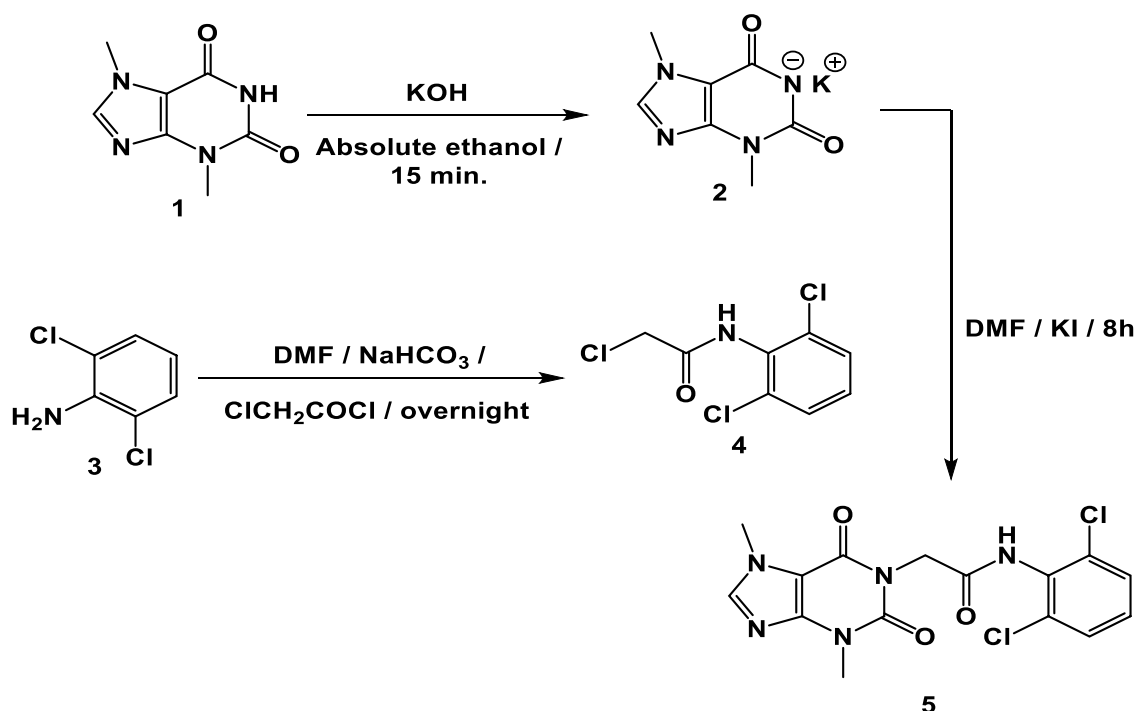
**Semi-synthesis of T-1-DOCA.** The procedure outlined in **Scheme 1** demonstrates the semi-synthetic process involved in the production of the target compound, **T-1-DOCA**. Initially, theobromine **1**, 3,7-dimethyl-3,7-dihydro-1H-purine-2,6-dione, was subjected to refluxing with alcoholic KOH, resulting in the formation of its potassium salt.<sup>45</sup> To obtain the required

intermediate compound, 2,6-dichloroaniline **3** and chloroacetylchloride were refluxed in DMF, utilizing NaHCO<sub>3</sub> as a base. This reaction yielded compound **4**. Subsequently, equimolar amounts of compounds **2** and **4** were refluxed in DMF, employing potassium iodide (sufficient amount) as a catalyst. This reaction successfully produced the desired end product, compound **5**, as expected.

Absorption bands at 3249 for NH, 1719, and 1660 cm<sup>-1</sup> for C=O have appeared in **T-1-DOCA**'s IR spectrum. Moreover, remarkable up-field signals corresponding to the 2 CH<sub>3</sub> groups of theobromine were observed in the <sup>1</sup>H NMR spectrum at 3.90 and 3.45 ppm. Additionally, at 4.80 ppm, a singlet signal for the 2 methylene protons could be seen. The <sup>13</sup>C NMR spectrum revealed 3 shielded signals at ppm 43.82 (for CH<sub>2</sub> carbon), 33.69, and 29.93 (for theobromine's 2 methyl carbons).

#### *Biological evaluation*

**In vitro EGFR inhibition.** In order to validate the proposed design and computational findings, we examined the potential of **T-1-DOCA** against the EGFR<sup>WT</sup> and EGFR<sup>T790M</sup> proteins in vitro. The inhibitory effects of **T-1-DOCA** were found to be significant, with IC<sub>50</sub> values of 56.94 and 269.01 nM, respectively (of erlotinib were 5.93 and 212.20 nM, respectively). These findings corroborate the in silico predictions, which suggested a strong potential for EGFR<sup>WT</sup> and EGFR<sup>T790M</sup> inhibition by **T-1-DOCA**. Therefore, it can be concluded that **T-1-DOCA** shows promising inhibitory activity against EGFR, both computationally and experimentally. Following, **T-1-DOCA** will be subjected to in vitro assessment for anticancer activities against different cell lines.



**Scheme 1.** The semi-synthetic procedure of **T-1-DOCA (5)**.

**Table 6.** The results of assessing the anti-proliferative properties of **T-1-NCA** against the HCT-116 and H1975 cell lines.

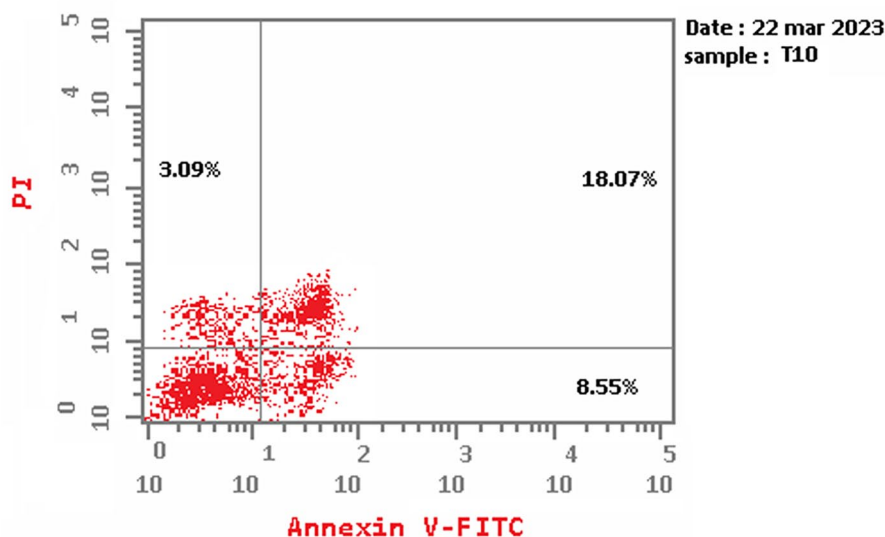
COMP.	HCT-116 IC <sub>50</sub> (μM)	H1975 IC <sub>50</sub> (μM)
<b>T-1-DOCA</b>	23.30	14.12
Erlotinib	17.92	-
Staurosporine	-	4.42

**Cytotoxicity.** Based on the inhibitory potentials demonstrated by **T-1-DOCA** against EGFR<sup>WT</sup> and EGFR<sup>T790M</sup> in both in silico and in vitro experiments, there is a strong possibility that this compound can exhibit promising anticancer effects. In order to investigate this potential, the cytotoxicity of **T-1-DOCA** was assessed against 2 different cancer cell lines, namely, non-small cell lung cancer H1975 and human colon cancer HCT-116, while using staurosporine and erlotinib as reference drugs, respectively. The results (Table 6) showed that **T-1-DOCA** exhibited a potent anticancer effect against these cancer cells, with IC<sub>50</sub> values of 14.12.84 and 23.30 μM, respectively. These values were comparable to those obtained for reference drugs, which had IC<sub>50</sub> values of 4.42 and 17.83 μM, respectively. To further explore the safety profile and specificity of **T-1-DOCA**, we conducted experiments using the normal Vero cell line. Interestingly, **T-1-DOCA** exhibited a high IC<sub>50</sub> value of 95.28 μM, indicating a low toxicity profile. Additionally, the compound demonstrated remarkably high selectivity indexes (SI) of 6.8 and 4.1 against the 2 cancer cell lines, which is a promising finding. These results suggest that **T-1-DOCA** has the potential to be a safe and effective anticancer drug with high specificity against cancer cells.

**Flow cytometric analysis of apoptosis.** Apoptosis is a highly regulated process of programmed cell death that helps to maintain a balance between the production and death of cells, which is essential for normal cellular homeostasis. Any disturbance in this balance can lead to a variety of pathological conditions such as autoimmune diseases and abnormal cell proliferation.<sup>62</sup> Apoptosis plays a vital role in various developmental processes, tissue regeneration, and eliminating inflammatory cells. In the 1980s, the induction of apoptosis became an important therapeutic strategy after the discovery of DNA breakage in thymocytes following exposure to glucocorticoids.<sup>5,63</sup> To evaluate the apoptotic potential of **T-1-DOCA**, the apoptosis percentage in the HCT-116 cells was determined using Annexin V and PI double stains.<sup>64</sup> The results (Table 7 and Figure 14) demonstrated that **T-1-DOCA** induced a significant increase in the percentage of apoptotic cells in the early stage of apoptosis (from 0.72 to 8.55), late stage of apoptosis (from 0.14 to 18.07), and the total percentage by almost 10 folds. The necrosis percentage was also increased compared to control cells (from 2.02 to 3.09). Overall, the results indicate that **T-1-DOCA** has promising anticancer properties and the potential to induce apoptosis in cancer cells. The ability of **T-1-DOCA** to induce

**Table 7.** The impact of **T-1-DOCA** on apoptosis in HCT-116 cells.

SAMPLE	APOPTOSIS			NECROSIS
	TOTAL	EARLY	LATE	
<b>T-1-DOCA</b>	29.71	8.55	18.07	3.09
Control cells	3.06	0.72	0.14	2.02

**Figure 14.** The impact of **T-1-DOCA** on the process of apoptosis in HCT-116 cells.**Table 8.** T-1-DOCA's potentials on apoptotic proteins.

SAMPLE	RT-PCR FOLD CHANGE			
	CASP3	CASP9	BAX	BCL-2
<b>T-1-DOCA-treated HCT-116 cells</b>	3.829	2.238	5.522	0.521
HCT-116 control cells	1	1	1	1

apoptosis could be an effective strategy in the development of new therapeutic agents for the treatment of cancer and other pathological conditions.

*Reverse transcription-polymerase chain reaction (RT-PCR).* The present study aimed to investigate the impact of **T-1-DOCA** on the expression of apoptosis-related proteins, including BAX, Bcl-2, caspase-3, and caspase-9, in HCT-116 cells to get a thorough evaluation of the apoptotic process. This multifaceted approach encompasses the critical balance between pro-apoptotic and anti-apoptotic factors, as well as the activation of key enzymes responsible for executing apoptosis. By scrutinizing these diverse aspects, we will gain a comprehensive understanding of how apoptosis is induced and regulated. The cells were treated with **T-1-DOCA** and the expression levels of the aforementioned proteins were compared to the control (untreated) group of cells employing the RT-PCR.<sup>65</sup> The

results showed that **T-1-DOCA** significantly affected the expression levels of these proteins, suggesting its potential as an apoptotic anti-cancer agent. BAX, a pro-apoptotic protein that plays a vital role in promoting cell apoptosis,<sup>66</sup> was found to increase by 5.5 times in **T-1-DOCA**-treated HCT-116 cells compared to the control (Table 8). On the other hand, the anti-apoptotic protein Bcl-2, which inhibits apoptosis and promotes cell survival,<sup>67</sup> was significantly reduced by 2-fold compared to the control. These findings suggest that **T-1-DOCA** promotes apoptosis in HCT-116 cells. Furthermore, **T-1-DOCA** was found to increase the levels of caspase-3 and caspase-9, which are crucial enzymes involved in apoptosis. Caspase-3 is an initiator caspase, and its activation marks the start of the apoptotic pathway.<sup>68</sup> In contrast, caspase-9 is an executioner caspase, and its activation occurs downstream in the pathway.<sup>69</sup> The significant increase in caspase-3 levels by 3.8-fold and caspase-9 levels by 2.2-fold in **T-1-DOCA**-treated HCT-116

cells compared to the control further supports its potential as an apoptosis promotor. The results of this study provide insights into the mechanism of action of **T-1-DOCA** as an anti-cancer agent and suggest that it may have therapeutic potential in the treatment of cancer.

## Experimental

### Docking studies

Docking studies have been administered for **T-1-DOCA** against EGFR<sup>WT</sup> (wild protein) and EGFR<sup>T790M</sup> (mutant protein) by MOE2014 software.<sup>70</sup> The Supplemental section includes an additional explanation and details about this study.

### MD simulations

MD simulations studies have been administered for the EGFR-**T-1-DOCA** complex by the CHARMM-GUI web server<sup>71</sup> and GROMACS 2021. The Supplemental section includes an additional explanation and details about this study.<sup>72,73</sup>

### MM-GBSA

MM-GBSA has been administered for EGFR-**T-1-DOCA** complex by the Gmx\_MMPBSA package.<sup>74,75</sup> The Supplemental section includes an additional explanation and details about this study.

### ED analysis

Principal Component Analysis (PCA) have been employed to EGFR-**T-1-DOCA** complex to investigate the alpha carbons' dynamic motion that located in the amino acid sequence spanning from Glu826 to Leu1161.<sup>76</sup> The Supplemental section includes an additional explanation and details about this study.

### Bi-dimensional assays

Bi-dimensional assays have been administered for EGFR-**T-1-DOCA** complex to compare frames within the reduced subspace, we merged, aligned, created a new C matrix, and plotted the projections.<sup>77</sup> The Supplemental section includes additional explanation and details about this study.

### DFT

DFT computations have been administered for **T-1-DOCA** by Gaussian 09 and GaussSum3.0 programs. The Supplemental section includes an additional explanation and details about this study.

### ADMET studies

ADMET profiling has been computationally administered for **T-1-DOCA** by Discovery Studio 4.0.<sup>78</sup> The Supplemental

section includes an additional explanation and details about this study.

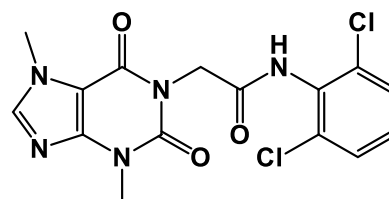
### Toxicity studies

Toxicity profiling has been computationally administered for **T-1-DOCA** by Discovery Studio 4.0. The Supplemental section includes an additional explanation and details about this study.

### Chemistry

*General procedure for the synthesis of T-1-DOCA.* The potassium 3,7-dimethyl-3,7-dihydro-1H-purine-2,6-dione **2** (0.001 mol, 0.25 g) in dry DMF (10 mL) solution was mixed with 2-Chloro-N-(2,6-dimethylphenyl)acetamide **4** (0.001 mol, 0.26 g), and the mixture was heated in a water bath for 5 h. The reaction mixture was added to 200 mL of ice water and gently stirred for 1 h. The obtained cake powder was filtered, water washed, and crystallized from methanol to produce the final compound **5** (**T-1-DOCA**).

*N-(2,6-Dichlorophenyl)-2-(3,7-dimethyl-2,6-dioxo-2,3,6,7-tetrahydro-1H-purin-1-yl)acetamide.*



Off-white powder (yield, 70%); m. p.=222–224°C; IR (KBr)  $\nu$  cm<sup>-1</sup>: 3249 (NH), 2966, 2926 (CH aliphatic), 1719, 1660 (C=O); <sup>1</sup>H NMR (400 MHz, DMSO-d<sub>6</sub>)  $\delta$  10.05 (s, 1H), 8.08 (s, 1H), 7.88 (m, 1H), 7.55 (m, 1H), 7.25 (m, 1H), 4.80 (s, 2H), 3.90 (s, 3H), 3.45 (s, 3H); <sup>13</sup>C NMR (101 MHz, DMSO-d<sub>6</sub>)  $\delta$  167.26, 154.59, 151.32, 149.00, 143.76, 136.27, 132.01, 131.41, 126.16, 124.78, 124.38, 107.02, 43.82, 33.69, 29.93; Mass (*m/z*): 382 (M<sup>+</sup>, 43%), and 267 (100%, base peak); Anal. Calcd. For C<sub>15</sub>H<sub>13</sub>Cl<sub>2</sub>N<sub>5</sub>O<sub>3</sub> (382.20): C, 47.14; H, 3.43; N, 18.32; Found: C, 47.30; H, 3.57; N, 18.49%.

### In vitro EGFR inhibition

The In vitro EGFR inhibition assay has been administered for **T-1-DOCA** by Human EGFR ELISA kit against EGFR<sup>WT</sup> (wild protein) and EGFR<sup>T790M</sup> (mutant protein).<sup>79</sup> The Supplemental section includes an additional explanation and details about this study.

### In vitro antiproliferative and safety activities

The In vitro antiproliferative activities have been administered for **T-1-DOCA** by MTT procedure.<sup>80,81</sup> The Supplemental section includes an additional explanation and details about this study.

### Flow cytometry of apoptosis

The Apoptosis incidence has been evaluated for **T-1-DOCA** through flow cytometry analysis technique.<sup>82</sup> The Supplemental section includes an additional explanation and details about this study.

### Rt-PCR assay

Levels of BAX, Bcl-2, caspase-3, and caspase-9 were investigated by RT-PCR using the kit (Qiagen RNA extraction/BioRad syber green PCR MMX). The Supplemental section includes an additional explanation and details about this study.

### Conclusion

In conclusion, this study aimed to design and evaluate a novel apoptotic EGFR inhibitor, **T-1-DOCA**, by utilizing the essential pharmacophoric structural properties of EGFR inhibitors. Computational techniques such as DFT computations, molecular docking, MD, MM-GPSA, and PLIP experiments were employed to evaluate the potential of **T-1-DOCA**. Prior to the semi-synthesis, **T-1-DOCA**'s computational ADME and toxicity profiles were also evaluated. The in vitro assays revealed that **T-1-DOCA** is a potent apoptotic EGFR inhibitor that exhibited significant efficacy in suppressing the proliferation of H1975 and HCT-116 malignant cell lines with selectivity indices of 1.8 and 4.1, respectively, indicating its potential as an anticancer agent with a favorable safety profile. Furthermore, **T-1-DOCA** was found to induce apoptosis by significantly increasing the levels of BAX, Casp3, and Casp9 and decreasing the levels of Bcl-2. In summary, **T-1-DOCA** is a promising candidate for further development as a safe and effective anti-cancer drug

### Author Contributions

The study was conceptualized and designed by IHE and AMM. AMM, HE, and EBK supervised the work. The semi-synthesis was performed by RGY and HE, while DZH, and IMI conducted the DFT and the MD studies, respectively. Biological investigations were carried out by HAE. The funding for the study was obtained by EBE and AAA, who also contributed to writing the manuscript. All authors have thoroughly reviewed and approved the final manuscript.

### Institutional Review Board Statement

Not applicable.

### Informed Consent Statement

Not applicable.

### ORCID iD

Ahmed M Metwaly  <https://orcid.org/0000-0001-8566-1980>

### Data Availability Statement

Upon request, the corresponding authors have access to the data and can provide it.

### Sample Availability

Upon request, **T-1-DOCA** can be provided from the authors.

### Supplemental Material

Supplemental material for this article is available online.

### REFERENCES

1. Curado MP, Voti L, Sortino-Rachou AM. Cancer registration data and quality indicators in low and middle income countries: their interpretation and potential use for the improvement of cancer care. *Cancer Causes Control*. 2009;20:751-756.
2. WHO. Cancer, Fact sheet. 2018. Accessed October 2018. <http://www.who.int/news-room/fact-sheets/detail/cancer>
3. Voss A, Strasser A. The essentials of developmental apoptosis. *F1000Res*. 2020; 9:F1000.
4. Jan R, Chaudhry GES. Understanding apoptosis and apoptotic pathways targeted cancer therapeutics. *Adv Pharm Bull*. 2019;9:205-218.
5. Carneiro BA, El-Deiry WS. Targeting apoptosis in cancer therapy. *Nat Rev Clin Oncol*. 2020;17:395-417.
6. Grant SK. Therapeutic protein kinase inhibitors. *Cell Mol Life Sci*. 2009;66: 1163-1177.
7. Normanno N, De Luca A, Bianco C, et al. Epidermal growth factor receptor (EGFR) signaling in cancer. *Gene*. 2006;366:2-16.
8. Huang S-M, Harari PM. Epidermal growth factor receptor inhibition in cancer therapy: biology, rationale and preliminary clinical results. *Investig New Drugs*. 1999;17:259-269.
9. Ciardiello F, Tortora G. EGFR antagonists in cancer treatment. *N Engl J Med*. 2008;358:1160-1174.
10. Huang L, Fu L. Mechanisms of resistance to EGFR tyrosine kinase inhibitors. *Acta Pharm Sin B*. 2015;5:390-401.
11. Nicholson RI, Gee JMW, Harper ME. EGFR and cancer prognosis. *Eur J Cancer*. 2001;37:9-15.
12. Alharbi KS, Javed Shaikh MA, Afzal O, et al. An overview of epithelial growth factor receptor (EGFR) inhibitors in cancer therapy. *Chem Biol Interact*. 2022; 366:108-110.
13. Tan S, Lu R, Yao D, et al. Identification of LRRK2 inhibitors through computational drug repurposing. *ACS Chem Neurosci*. 2023;14:481-493.
14. Deng JN. Computer-aided drug design. *Current Drug Synthesis*. Wiley; 2023; 339-372.
15. Lin X, Li X, Lin X. A review on applications of computational methods in drug screening and design. *Molecules*. 2020;25:1375.
16. da Rosa R, Schenkel EP, Campos Bernardes LS. Semisynthetic and newly designed derivatives based on natural chemical scaffolds: moving beyond natural products to fight *Trypanosoma cruzi*. *Phytochem Rev*. 2020;19:105-122.
17. McCardle K, Pan J. Computational chemistry for all. *Nat Comput Sci*. 2022;2: 134-136.
18. Anesthessia B. *Coming of Age in the World of Modern In Silico Drug Design*. Lippincott Williams & Wilkins; 2023:129-131.
19. Cohen NC. *Guidebook on Molecular Modeling in Drug Design*. Gulf Professional Publishing; 1996.
20. Keith JA, Vassilev-Galindo V, Cheng B, et al. Combining machine learning and computational chemistry for predictive insights into chemical systems. *Chem Rev*. 2021;121:9816-9872.
21. Chalkha M, Nakkabi A, Hadda TB, et al. Crystallographic study, biological assessment and POM/Docking studies of pyrazoles-sulfonamide hybrids (PSH): Identification of a combined antibacterial/antiviral pharmacophore sites leading to in-silico screening the anti-Covid-19 activity. *J Mol Struct*. 2022; 1267:133605-133608.
22. Pracht P, Bohle F, Grimme S. Automated exploration of the low-energy chemical space with fast quantum chemical methods. *Phys Chem Chem Phys*. 2020;22: 7169-7192.
23. Moroy G, Martiny VY, Vayer P, Villoutreix BO, Miteva MA. Toward in silico structure-based ADMET prediction in drug discovery. *Drug Discov Today*. 2012;17:44-55.
24. Tielens F, Gierada M, Handzlik J, Calatayud M. Characterization of amorphous silica based catalysts using DFT computational methods. *Catal Today*. 2020;354:3-18.
25. Hollingsworth SA, Dror RO. Molecular dynamics simulation for all. *Neuron*. 2018;99:1129-1143.
26. Liu X, Shi D, Zhou S, et al. Molecular dynamics simulations and novel drug discovery. *Expert Opin Drug Discov*. 2018;13:23-37.
27. Hansson T, Oostenbrink C, van Gunsteren W. Molecular dynamics simulations. *Curr Opin Struct Biol*. 2002;12:190-196.
28. Fogli S, Polini B, Del Re M, et al. EGFR-TKIs in non-small-cell lung cancer: focus on clinical pharmacology and mechanisms of resistance. *Pharmacogenomics*. 2018;19:727-740.

29. Sun R, Hou Z, Zhang Y, Jiang B. Drug resistance mechanisms and progress in the treatment of EGFR-mutated lung adenocarcinoma. *Oncol Lett.* 2022;24:408.
30. Liu Q, Yu S, Zhao W, et al. EGFR-TKIs resistance via EGFR-independent signaling pathways. *Mol Cancer.* 2018;17:53.
31. Feng L, Gu J, Yang Y, Yang B, Shi R. Editorial: Exploring the therapeutic effects of synthetic, semi-synthetic and naturally derived compounds against cancer. *Front Pharmacol.* 2023;14:14-15.
32. Becker A, van Wijk A, Smit EF, Postmus PE. Side-effects of long-term administration of erlotinib in patients with non-small cell lung cancer. *J Thorac Oncol.* 2010;5:1477-1480.
33. Galimont-Collen AF, Vos LE, Lavrijsen AP, Ouwerkerk J, Gelderblom H. Classification and management of skin, hair, nail and mucosal side-effects of epidermal growth factor receptor (EGFR) inhibitors. *Eur J Cancer.* 2007;43:845-851.
34. Ayati A, Moghimi S, Salarinejad S, et al. A review on progression of epidermal growth factor receptor (EGFR) inhibitors as an efficient approach in cancer targeted therapy. *Bioorg Chem.* 2020;99:103811-103817.
35. Zhao Z, Wu H, Wang L, et al. Exploration of type II binding mode: a privileged approach for kinase inhibitor focused drug discovery? *ACS Chem Biol.* 2014;9:1230-1241.
36. Furet P, Caravatti G, Lydon N, et al. Modelling study of protein kinase inhibitors: binding mode of staurosporine and origin of the selectivity of CGP 52411. *J Comput Aided Mol Des.* 1995;9:465-472.
37. Gandin V, Ferrarese A, Dalla Via M, et al. Targeting kinases with anilino-pyrimidines: discovery of N-phenyl-N'-[4-(pyrimidin-4-ylamino)phenyl]urea derivatives as selective inhibitors of class III receptor tyrosine kinase subfamily. *Sci Rep.* 2015;5:16750-16762.
38. Liu Y, Gray NS. Rational design of inhibitors that bind to inactive kinase conformations. *Nat Chem Biol.* 2006;2:358-364.
39. Wheeler DL, Dunn EF, Harari PM. Understanding resistance to EGFR inhibitors-impact on future treatment strategies. *Nat Rev Clin Oncol.* 2010;7:493-507.
40. Moore M, Goldstein D, Hamm J, et al. Erlotinib plus gemcitabine compared with gemcitabine alone in patients with advanced pancreatic cancer: a phase III trial of the National Cancer Institute of Canada Clinical Trials Group. *J Clin Oncol.* 2007;25:1960-1966.
41. Wu SG, Liu Y-N, Tsai M-F, et al. The mechanism of acquired resistance to irreversible EGFR tyrosine kinase inhibitor-afatinib in lung adenocarcinoma patients. *Oncotarget.* 2016;7:12404-12413.
42. Wecker H, Waller C. Afatinib. *Small Mol Oncol.* 2018;199-215.
43. Metwaly AM, Lianlian Z, Luqi H, Deqiang D. Black ginseng and its saponins: preparation, phytochemistry and pharmacological effects. *Molecules.* 2019;24:1856-1871.
44. Metwaly AM, Ghoneim MM, Eissa IH, et al. Traditional ancient Egyptian medicine: a review. *Saudi J Biol Sci.* 2021;28:5823-5832.
45. Elkaeed EB, Yousef RG, Elkady H, et al. New anticancer theobromine derivative targeting egfrwt and egfrrt790m: design, semi-synthesis, in silico, and in vitro anticancer studies. *Molecules.* 2022;27:5859.
46. Elkaeed E, Yousef R, Elkady H, et al. A new theobromine-based EGFRWT and EGFR790M inhibitor and apoptosis inducer: design, semi-synthesis, Docking, DFT, MD simulations, and in vitro studies. *Processes.* 2022;10:2290.
47. Hisham M, Youssif BGM, Osman EEA, Hayallah AM, Abdel-Aziz M. Synthesis and biological evaluation of novel xanthine derivatives as potential apoptotic antitumor agents. *Eur J Med Chem.* 2019;176:117-128.
48. Sobh EA, Dahab MA, Elkaeed EB, et al. Computer aided drug discovery (CADD) of a thieno[2,3-d]pyrimidine derivative as a new EGFR inhibitor targeting the ribose pocket. *J Biomol Struct Dyn.* 2023;1-23. doi:10.1080/07391102.2023.2204500
49. Eissa IH, G.Yousef R, Elkady H, et al. New apoptotic anti-triple-negative breast cancer theobromine derivative inhibiting EGFRWT and EGFR790M: in silico and in vitro evaluation. *Mol Divers.* 2023;1-21.
50. Elzahabi HSA, Nossier ES, Alasfoury RA, et al. Design, synthesis, and anticancer evaluation of new pyrido[2,3-d]pyrimidin-4(3H)-one derivatives as potential EGFRWT and EGFR790M inhibitors and apoptosis inducers. *J Enzym Inhib Med Chem.* 2022;37(1):1053-1076.
51. Eissa IH, Yousef RG, Elkady H, et al. A new anticancer semisynthetic theobromine derivative targeting EGFR protein: CADD study. *Life.* 2023;13:191.
52. Eissa IH, Yousef RG, Elkaeed EB, et al. Anticancer derivative of the natural alkaloid, theobromine, inhibiting EGFR protein: computer-aided drug discovery approach. *PLoS One.* 2023;18(3):e0282586.
53. Husein DZ, Hassanien R, Khamis M. Cadmium oxide nanoparticles/graphene composite: synthesis, theoretical insights into reactivity and adsorption study. *RSC Adv.* 2021;11:27027-27041.
54. Wang T, Husein DZ, Research P. Novel synthesis of multicomponent porous nano-hybrid composite, theoretical investigation using DFT and dye adsorption applications: disposing of waste with waste. *Environ Sci Pollut Res.* 2022;30:8928-8955.
55. Nossier ES, Alasfoury RA, Hagra M, et al. Modified pyrido[2,3-d]pyrimidin-4(3H)-one derivatives as EGFRWT and EGFR790M inhibitors: design, synthesis, and anti-cancer evaluation. *J Mol Struct.* 2022;1270:133971-133986.
56. Eldehna WM, El Hassab MA, Elsayed ZM, et al. Design, synthesis, in vitro biological assessment and molecular modeling insights for novel 3-(naphthalen-1-yl)-4,5-dihydropyrazoles as anticancer agents with potential EGFR inhibitory activity. *Sci Rep.* 2022;12:12821-12913.
57. Lipinski CA, Lombardo F, Dominy BW, Feeney PJ. Experimental and computational approaches to estimate solubility and permeability in drug discovery and development settings. *Adv Drug Deliv Rev.* 1997;23:3-25.
58. Chuang KV, Gunsalus LM, Keiser MJ. Learning molecular representations for medicinal chemistry: miniperspective. *J Med Chem.* 2020;63:8705-8722.
59. Veber DF, Johnson SR, Cheng H-Y, et al. Molecular properties that influence the oral bioavailability of drug candidates. *J Med Chem.* 2002;45:2615-2623.
60. Idakwo G, Luttrell J, Chen M, et al. A review on machine learning methods for *in silico* toxicity prediction. *J Environ Sci Health C Environ Carcinog Ecotoxicol Rev.* 2018;36:169-191.
61. Kruhlak NL, Benz RD, Zhou H, Colatsky TJ. (Q)SAR modeling and safety assessment in regulatory review. *Clin Pharmacol Ther.* 2012;91:529-534.
62. Obeng E. Apoptosis (programmed cell death) and its signals - a review. *Braz J Biol.* 2021;81:1133-1143.
63. Wylie AH. Glucocorticoid-induced thymocyte apoptosis is associated with endogenous endonuclease activation. *Nature.* 1980;284:555-556.
64. Alanazi MM, Eissa IH, Alsaif NA, et al. Design, synthesis, docking, ADMET studies, and anticancer evaluation of new 3-methylquinoxaline derivatives as VEGFR-2 inhibitors and apoptosis inducers. *J Enzym Inhib Med Chem.* 2021;36:1760-1782.
65. Estus S. Optimization and validation of RT-PCR as a tool to analyze gene expression during apoptosis. In: Poirier J (ed.) *Apoptosis Techniques and Protocols.* *Neuromethods.* Humana Press; 1997:67-84.
66. Lalier L, Cartron P-F, Juin P, et al. Bax activation and mitochondrial insertion during apoptosis. *Apoptosis.* 2007;12:887-896.
67. Czabotar PE, Lessene G, Strasser A, Adams JM. Control of apoptosis by the BCL-2 protein family: implications for physiology and therapy. *Nat Rev Mol Cell Biol.* 2014;15:49-63.
68. Porter AG, Jänicke RU. Emerging roles of caspase-3 in apoptosis. *Cell Death Differ.* 1999;6:99-104.
69. Li P, Zhou L, Zhao T, et al. Caspase-9: structure, mechanisms and clinical application. *Oncotarget.* 2017;8:23996-24008.
70. Suleimen YM, Jose RA, Mamytbekova GK, et al. Isolation and in silico inhibitory potential against SARS-CoV-2 RNA polymerase of the rare kaempferol 3-O-(6"-O-acetyl)-Glucoside from *Calligonum tetrapterum*. *Plants.* 2022;11:2072.
71. Abraham MJ, Murtola T, Schulz R, et al. GROMACS: high performance molecular simulations through multi-level parallelism from laptops to supercomputers. *SoftwareX.* 2015;1-2:19-25.
72. Brooks BR, Brooks CL, Mackerell AD, et al. CHARMM: the biomolecular simulation program. *J Comput Chem.* 2009;30:1545-1614.
73. Jo S, Cheng X, Islam S, et al. CHARMM-GUI PDB manipulator for advanced modeling and simulations of proteins containing nonstandard residues. *Adv Protein Chem Struct Biol.* 2014;96:235-265.
74. Tuccinardi T. What is the current value of MM/PBSA and MM/GBSA methods in drug discovery? *Expert Opin Drug Discov.* 2021;16:1233-1237.
75. Valdés-Tresanco MS, Valdés-Tresanco ME, Valiente PA, Moreno E. gmx\_MMPBSA: a new tool to perform end-state free energy calculations with GROMACS. *J Chem Theory Comput.* 2021;17:6281-6291.
76. Amadei A, Linssen ABM, Berendsen HJC. Essential dynamics of proteins. *Proteins.* 1993;17:412-425.
77. Papaleo E, Mereghetti P, Fantucci P, Grandori R, De Gioia L. Free-energy landscape, principal component analysis, and structural clustering to identify representative conformations from molecular dynamics simulations: the myoglobin case. *J Mol Graph Model.* 2009;27:889-899.
78. Biovia DS. *Discovery Studio Modeling Environment.* Release; 2017.
79. Varkondi E, Schäfer E, Bökönyi G, et al. Comparison of ELISA-based tyrosine kinase assays for screening EGFR inhibitors. *J Recept Signal Transduct Res.* 2005;25:45-56.
80. Alley M, Scudiero D, Monks A, et al. Feasibility of drug screening with panels of human tumor cell lines using a microculture tetrazolium assay. *Cancer Res.* 1988;48:589-601.
81. van de Loosdrecht AA, Beelen RHJ, Ossenkoppele GJ, Broekhoven MG, Langenhuijsen MMAC. A tetrazolium-based colorimetric MTT assay to quantitate human monocyte mediated cytotoxicity against leukemic cells from cell lines and patients with acute myeloid leukemia. *J Immunol Methods.* 1994;174:311-320.
82. Wlodkovic D, Skommer J, Darzynkiewicz Z. Flow cytometry-based apoptosis detection. *Methods Mol Biol.* 2009;19-32.